

Full characterization of a carbon nanotube parallel double quantum dot

Gulibusitan Abulizi,^{1,*} Andreas Baumgartner,¹ and C. Schönenberger¹

¹*Department of Physics, University of Basel, Klingelbergstrasse 82, CH-4056 Basel, Switzerland*

We have measured the differential conductance of a parallel carbon nanotube (CNT) double quantum dot (DQD) with strong inter-dot capacitance and inter-dot tunnel coupling. Nominally, the device consists of a single CNT with two contacts. However, we identify two sets of Coulomb blockade (CB) diamonds that do not block transport individually, which suggest that two quantum dots (QDs) are contacted in parallel. We find strong and periodic anti-crossings in the gate and bias dependence, which are only possible if the QDs have similar characteristics. We discuss qualitatively the level spectrum and the involved transport processes in this device and extract the DQD coupling parameters. These results lead us to believe that clean and undoped QDs are formed parallel to the CNT axis, possibly on the outer and inner shells of a multi-wall CNT, or in a double-stranded CNT bundle.

INTRODUCTION

Recently, carbon nanotubes (CNTs) have been used as central elements in a variety of novel electronic devices, owing to their unique electrical and mechanical properties and compatibility with various material types and experimental setups [1–6]. There are many different types of CNTs [1], for example, metallic or semiconducting CNTs. Single-wall CNTs (SWCNTs) are a single sheet of rolled up graphene, while multi-wall CNTs (MWCNTs) consist of several coaxial CNTs of different diameters [7, 8]. In contrast, CNT bundles are a set of separate non-coaxial CNTs in parallel. Long metallic SWCNTs are promising systems, for example, to study one-dimensional Luttinger liquids [9], or novel quasi-particles with non-Abelian statistics [10]. SWCNTs of finite length are very reliable in showing size quantization of the energy levels, shell filling effects and Coulomb blockade (CB) in quantum dots (QDs). In comparison to QDs in SWCNTs, MWCNT QDs typically exhibit more complex electronic properties due to more available orbital states, which increase not only the number of conducting channels but also the possibility of intershell interactions [11].

Double QDs (DQDs) are versatile structures that exhibit many physically relevant phenomena [12]. DQDs in series between a source and a drain contact have been investigated regularly [13, 14], also in CNTs [15–17], for example, to investigate spin-blockade [18–20] and quantum bits [21]. In parallel DQDs, CB suppresses the electronic transport only if both dots are in blockade. This allows in principle for a more detailed characterization of the individual QDs and the effects of the coupling between the QDs by first order transport processes. However, parallel DQDs are investigated less frequently [22] and are more difficult to obtain on CNTs than DQDs in series, because of the close proximity between two CNTs that is required to obtain an appreciable tunnel coupling. Parallel DQDs can in principle form in MWCNTs, where separate QDs might form on different shells, or in non-overlapping parallel CNTs in a bundle, as depicted in

Fig. 1(a) and Fig. 1(b), respectively. However, if the tunnel coupling is very strong, we expect that the QD states are strongly hybridized and result in the increased degeneracies and shell filling effects typical for MWCNTs [23, 24]. In contrast, for very small couplings between the concentric CNTs two individual QD characteristics are expected. For intermediate couplings one might expect a hybridization that retains most of the characteristics of the individual QD states, while a pronounced anti-crossing occurs when two charge states become degenerate. Recently, anti-crossings have been observed in a CNT bundle [25], where two or more QDs of very different characteristics have formed. It is difficult in CNT DQDs to gate the QDs individually, so that the DQD characteristics have to be observed in the conductance measured as a function of the bias and a global backgate (BG).

Here, we report differential conductance measurements on a CNT device with two contacts and a global BG at cryogenic temperatures, for which we find two interpenetrating sets of CB diamonds with excited states and strong anti-crossings between specific resonances. These findings are consistent with two strongly coupled parallel QDs in a MWCNT or a tight double-stranded CNT bundle.

DEVICE FABRICATION

CNTs on substrates often suffer from potential variations on the substrate or residues from the contact fabrication after the CNT growth [26, 27] and cannot be cleaned by current annealing. Here, we employ a stamping method in which CNTs are grown on a separate wafer [28, 29] and are later transferred mechanically to the device substrate. The key advantage of CNT stamping techniques is to separate the CNT growth from the fabrication of markers and bonding pads [30]. A monolayer chemical vapor deposition (CVD) grown hexagonal boron nitride (hBN) is transferred on top of the CNTs to form a tunnel barrier between the CNTs and the metallic leads.

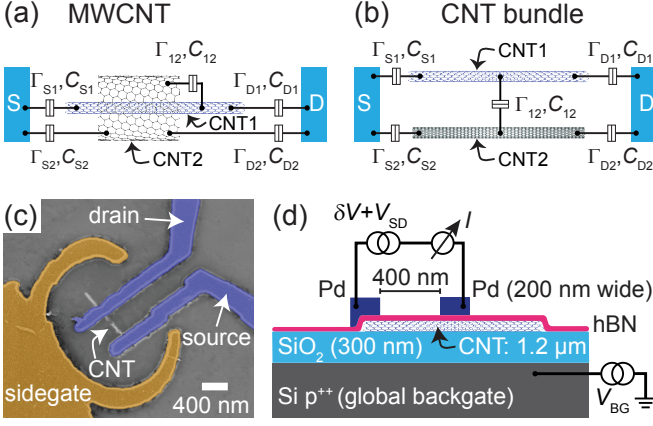


FIG. 1: Schematic illustration of a parallel-coupled DQDs formed (a) in a MWCNT, or (b) in a CNT bundle. (c) False-color SEM image of a two-terminal CNT device. The CNT is connected to the source and drain electrodes shown in blue and the sidegate shown in orange. (d) Schematic device cross section illustrating the device geometry and electronic setup.

We note that by depositing the hBN layer directly onto the stamped CNTs protects the CNTs from direct exposure to the resist or solvents, which would otherwise contaminate the active structure [31, 32]. Since the hBN layer thickness is small, we believe that the main effect is to reduce the adhesion of residues on the hBN, rather than to increase the distance between the CNTs and the scatterers on the surface.

The device fabrication starts with the manufacturing of the CNT stamps. A silicon (Si) substrate capped by a thermal oxide (SiO_2) layer is patterned into an array of square mesas using electron-beam lithography. Each mesa is $50\text{ }\mu\text{m}$ long and wide and $4\text{ }\mu\text{m}$ high, with a spacing of $50\text{ }\mu\text{m}$ between neighboring squares. After spin coating of Fe/Mo catalyst particles onto the mesas, we grow CNTs at 950°C for 10 minutes in a CVD process with methane as carbon precursor gas. The target substrate is a piece of a heavily p-doped Si wafer with 300 nm thick SiO_2 on top, which acts as a global BG. This substrate is patterned with $5\text{ nm}/45\text{ nm}$ Ti/Au markers and bonding pads. We then transfer the CNTs from the mesa substrate onto the target substrate using a mask aligner, by which the mesa and the target substrates are roughly aligned using the markers and pressed together. About $6 - 10$ CNTs are transferred to a $200 \times 200\text{ }\mu\text{m}^2$ area on average. We locate the CNTs using a scanning electron microscope (SEM) [32]. Immediately after this step a monolayer CVD hBN (from Graphene Supermarket) is transferred by a wet-etch process from its growth substrate to the target substrate [33] with the CNTs below. Thermal annealing at 200°C for 2 hours removes the poly(methyl methacrylate) (PMMA) resist residues on top of the transferred hBN layer [34]. Suitable CNTs are then contacted by $10\text{ nm}/50\text{ nm}$ Cr/Pd source and

drain contacts using electron-beam lithography.

An SEM image of the resulting device is shown in Fig. 1(c), and a schematic cross section with details of the device geometry and the electrical measurement setup is shown in Fig. 1(d). A $1.2\text{ }\mu\text{m}$ long CNT is contacted by 200 nm wide electrodes, separated by 400 nm . One contact (source) covers the end of the CNT, while the other (drain) does not. In this device a circular sidegate (SG) is fabricated in the same step for additional tunability. The sidegate voltage is kept constant for this work and will not be discussed further.

ELECTRICAL CHARACTERIZATION

At room temperature the device has a resistance of $5\text{ M}\Omega$ for negative gate voltages ($V_{\text{BG}} \approx -2\text{ V}$). Low-temperature transport properties are characterized in a ^3He refrigerator at a base temperature of $\sim 245\text{ mK}$. We apply a dc and an ac bias, $V_{\text{SD}} + \delta V$, to one contact (source) and measure the differential conductance $G = \delta I / \delta V$ of the device using standard lock-in techniques with an ac voltage of $\delta V = 40\text{ }\mu\text{V}$ at a frequency of 328 Hz , as illustrated in Fig. 1(d).

Figure 2(a) shows a colorscale plot of G as a function of V_{BG} and V_{SD} . We find a periodic pattern of strongly distorted CB diamonds, suggesting the formation of QDs in the CNT. While the weak CB diamond boundaries with positive slopes are straight, the ones with negative slopes consist of a series of avoided crossings. These lines have a larger amplitude, especially at larger bias, can be rather wide and can even occur in pairs.

To characterize the QDs formed in the device, we focus on the region pointed out by the dashed rectangle, with the corresponding data replotted in Fig. 2(b), while in Fig. 2(c) the positions of the resonances R1, R2 and R3 of Fig. 2(b) are plotted as solid red lines. First we identify individual CB diamonds and ignore the avoided crossings and other effects discussed below. For this we extrapolate the resonance position around zero bias, which results in the dashed black and blue diamonds. This two-QD pattern is shown exemplarily in Fig. 2(c), but also describes roughly the extended data set of Fig. 2(a). We therefore conclude that two QDs are formed in the system.

From these extrapolated CB diamonds we estimate the charging energies of the two individual QDs as $E_{\text{C1}} \approx 10.4\text{ meV}$ and $E_{\text{C2}} \approx 3.0\text{ meV}$, which correspond to the total capacitances $C_{\text{tot1}} \approx 15\text{ aF}$ and $C_{\text{tot2}} \approx 53\text{ aF}$, respectively. We label the QD with the larger charging energy as QD1 and the other as QD2. In the constant interaction model [35] the positive and negative slopes of an individual CB diamond are given by $+\frac{C_{\text{BG}}}{C_{\text{tot}} - C_{\text{S}}}$ and $-\frac{C_{\text{BG}}}{C_{\text{S}}}$, with $C_{\text{tot}} = C_{\text{BG}} + C_{\text{S}} + C_{\text{D}}$. From these expressions we obtain the capacitances listed in Table I for the individual QDs. Here, we neglect the inter-dot capacitance, which might explain the small discrepancies

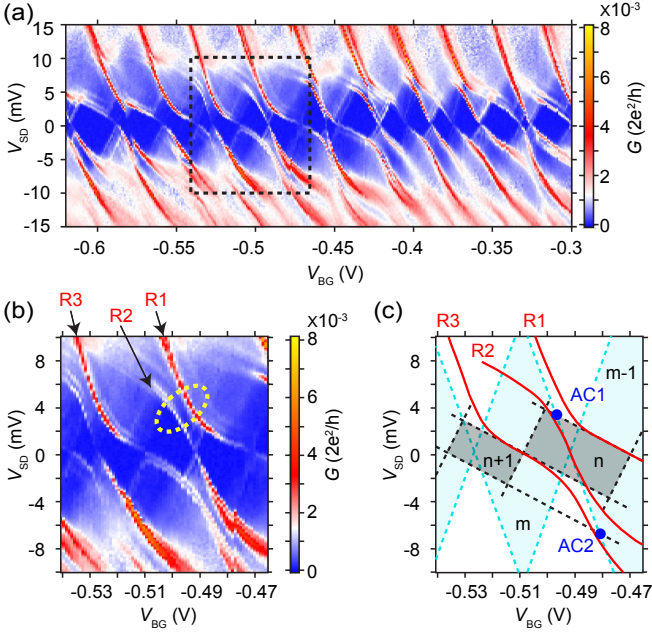


FIG. 2: (a) Colorscale plot of the differential conductance G as a function of V_{BG} and V_{SD} for a fixed SG voltage $V_{SG} = -2$ V and at $T = 245$ mK. (b) Magnification of the region indicated in Fig. 2(a). Three resonances are labeled as R1, R2, and R3. The yellow dashed ellipse highlights an avoided crossing. (c) Schematic charge stability diagram of the parallel DQDs extracted from Fig. 2(b). The three solid red lines correspond to the transport resonances (R1, R2, and R3) marked in Fig. 2(b) and the dashed lines are the extrapolated lines that separate the charge states of the individual QDs. AC1 and AC2 point out two avoided crossings, while n and m are the number of holes in the respective charge states.

in the sums from the measured C_{tot} . We find very similar values for the capacitive coupling of the drain to both QDs, for the BG to both QDs, and for the source to QD1. However, C_S of QD2 is about 8 times larger, possibly related to the fact that this is the contact that overlaps the end of the CNT. We note that both BG capacitances are virtually identical. In addition, we can use the full width at half maximum of the zero-bias resonances as upper limits for the tunnel coupling strengths, yielding $\Gamma_1 \leq 460 \mu\text{eV}$ and $\Gamma_2 \leq 305 \mu\text{eV}$, respectively.

TABLE I: Extracted parameters for QD1 and QD2.

parameters	QD1 (blue lines)	QD2 (black lines)
C_{tot}	15.3 aF	53.3 aF
C_{BG}	5.0 aF	5.3 aF
C_S	8.1 aF	41.0 aF
C_D	2.6 aF	6.0 aF
Γ	460 μeV	305 μeV
C_{12}	~ 5 aF	
Γ_{12}	$\geq 500 \mu\text{eV}$	

Figure 2(a) also shows excited state resonances, which run in parallel to the CB diamond boundaries. These lines are most pronounced for the resonances with negative slopes, which suggest fairly asymmetric tunnel barriers [35]. We extract the mean energy difference between these resonances as $\delta E \approx 0.9$ meV. If we assume the confinement length L to be the 400 nm spacing between the source and drain electrodes, we expect a mean level spacing $\delta E = \hbar v_F / 2L \approx 4$ meV for an ideal and undoped metallic CNT, with \hbar the Planck constant and $v_F = 8 \times 10^5$ m/s the Fermi velocity [36]. This expected value is a factor of four larger than the energy difference between the excited states in Fig. 2(a), suggesting both QDs are considerably larger than the contact spacing. Though we might overestimate the level spacing in case of a semiconducting CNT because of the flat electronic band structure close to the band gap [37], we speculate that by introducing a monolayer hBN tunnel barrier between the selected CNT and the metal contacts, it is possible that a larger QD forms on the significantly longer CNT, because the contacts are weakly coupled and do not necessarily result in electron confinement. As a result, the QD wave function can extend beyond the spacing between the source and drain contacts for weakly coupled tunnel contacts (hBN layer).

We now turn to the discussion of the avoided crossings shown for example in Fig. 2(b), where the avoided crossing AC1 is highlighted by a yellow dashed ellipse. An avoided crossing is observed at the intersection points between the CB diamond boundaries of QD1 and QD2 with negative slopes. This can be understood easily by considering that at these points the chemical potentials ("resonances") of both QDs would both be aligned with the electrochemical potential of the drain ($\mu_D = 0$), which means that both QD potentials are identical and electrons (or holes) can be exchanged not only with the leads, but also between the QDs. This results in a hybridization of the QD wave functions and an avoided crossing in their spectrum. The increased resonance amplitudes can be understood qualitatively in the sequential tunneling picture by considering the case $\Gamma_{12} \gg \Gamma_j$, where j stands for all the contacts. As illustrated in Fig. 3(a) the DQD then acts like a single QD with 4 leads. In addition to the paths through the individual QDs, electrons (or holes) can also tunnel into one QD and out of the other, which can result in more than the sum of the currents through the individual QDs. The total tunneling rate reads $\Gamma = (\Gamma_{S1} + \Gamma_{S2})(\Gamma_{D1} + \Gamma_{D2}) / \Gamma_\Sigma = (\Gamma_{S1}\Gamma_{D1} + \Gamma_{S2}\Gamma_{D2} + \Gamma_{S2}\Gamma_{D1} + \Gamma_{S1}\Gamma_{D2}) / \Gamma_\Sigma$ with $\Gamma_\Sigma \approx \Gamma_{S1} + \Gamma_{S2} + \Gamma_{D1} + \Gamma_{D2}$. The first two terms are essentially the individual QD transmissions, which are dominated by the last two terms for the situation of very asymmetric couplings shown in Fig. 3(a). We would in principle expect a similar effect for the CB resonances with positive slopes (the dot potentials aligned with the source Fermi energy). However, since the two positive slopes are very

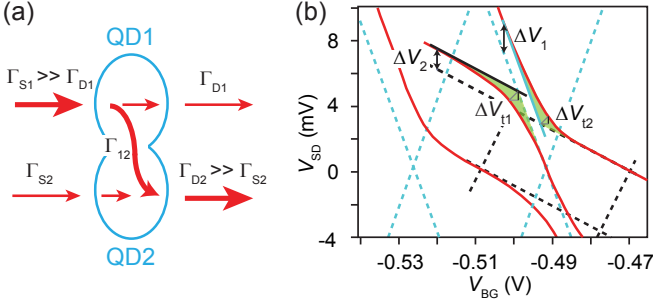


FIG. 3: (a) Schematic sequential tunneling through a strongly coupled DQD. (b) Replot of the charge stability diagram in Fig. 2(c) with the focus on the avoided crossing AC1 discussed in the text.

similar, no such crossing is observed on this device.

To characterize the avoided crossings, we replot the positions of the three resonance curves R1, R2 and R3 in Fig. 3(b) and focus on the avoided crossing AC1. We now draw the asymptotes to the resonances away from AC1. Two lines are the CB diamond edges found above, but the other two are offset in bias by ΔV_1 and ΔV_2 , respectively. These offsets are in analogy with the zero-bias gate maps in more standard, separately gated DQDs in series [12]. The offsets are due to one QD capacitively sensing the charge state of the other, while the bending of the resonances, indicated as green shadings in Fig. 3(b), stems from the inter-dot tunnel coupling.

We first extract the inter-dot capacitance C_{12} from the resonance offsets: the addition of one electron to QD i results in a change of the electrical potential in QD j , $\Delta\Phi_j$ (and vice versa), due to the capacitive coupling. For $C_{12} \ll C_{\text{tot}1}, C_{\text{tot}2}$ one finds $\Delta\Phi_j = \frac{e^2}{C_{\text{tot}1}C_{\text{tot}2}}C_{12}$. This shift in the potential has to be compensated by a change $\Delta V_{\text{SD}}^{(j)}$ in the bias measured between the two asymptotes corresponding to QD j . For the drain resonance one obtains $0 = \Delta\Phi_j + e\alpha_{Sj}\Delta V_{\text{SD}}$ with the source lever arm $\alpha_{Sj} = \frac{C_{Sj}}{C_{\text{tot}j}}$. From this, one directly obtains:

$$C_{12} = -\frac{C_{\text{tot}i}C_{Sj}}{e}\Delta V_{\text{SD}}^{(j)} \quad (1)$$

Similarly, from the the resonance condition at the source contact, $e\Delta V_{\text{SD}}^{(j)} = \Delta\Phi_j + e\alpha_{Sj}\Delta V_{\text{SD}}^{(j)}$, one then obtains $C_{12} = \frac{1}{e}C_{\text{tot}i}(C_{\text{tot}j} - C_{Sj})\Delta V_{\text{SD}}^{(j)}$. Inserting the experimental values for the offsets $\Delta V_{\text{SD}}^{(j)}$ and the capacitances in Table I, we find consistently for both QD resonance lines at AC1 the inter-dot capacitance $C_{12} \approx 5$ aF. Interestingly, this value varies between 5 aF and 9 aF for four neighboring avoided crossings, which might be either due to other crossings nearby (here, for example AC2), or a deeper reason, possibly due to the QD quantum capacitance that might change with the charge and orbital states, and with the bias. The extracted value is comparable to the gate and contact capacitances, so that

this value has to be taken as an approximation.

We estimate the inter-dot tunnel coupling strength by considering only the bias component of the bending, ΔV_t , as illustrated in Fig. 3(b). This results in a lower limit for the tunnel coupling, $\Gamma_{12} \geq 500 \mu\text{eV}$. We note that we find a rather large variation ($\sim 20\%$) between the extracted values for different avoided crossings, which probably originates from errors in the asymptotic lines. We point out that this value is of similar strength as the total tunnel coupling to the leads.

One might expect that with the inter-dot coupling parameters one should be able to distinguish whether the DQD is formed on two shells of a MWCNT or on two separate CNTs in a bundle, see Fig. 1(a) and Fig. 1(b), respectively. The expressions for the capacitances of two parallel or coaxial cylinders at a distance compatible with a large inter-dot tunnel coupling (few nanometers) both suggest unphysically small CNT diameters. The reason for this is that the source and drain contacts reduce the inter-dot capacitance due to screening, which can only be accounted for numerically [32]. However, two parallel CNTs in a bundle would naturally account for the identical gate capacitances of the two QDs.

CONCLUSIONS

We report low-temperature differential conductance measurements on parallel DQDs, formed on two shells of a MWCNT or on two individual CNTs of a bundle. We investigate avoided crossings that result from the tunnel and capacitive couplings between the electronic charge states of different QDs. Our results enrich the fundamental understanding of quantum transport through coupled QDs formed in a parallel configuration. We demonstrate that in the sense of the simplest DQD model (large level spacing and constant interaction), transport spectroscopy can be used as a sensitive tool to fully characterize the interactions between parallel-coupled QDs also in a two-terminal CNT device with only a single global gate.

ACKNOWLEDGEMENTS

We thank T. Hasler and K. Thodkar for their help with the CNT stamps and the hBN transfer process, respectively. This work was financially supported by the Swiss National Science Foundation (SNF), the Swiss Nanoscience Institute (SNI), the Swiss NCCR QSIT, and the European ERC project QUEST.

* Electronic address: gulibusitan.abulizi@unibas.ch

- [1] E. A. Laird, F. Kuemmeth, G. A. Steele, K. Grove-Rasmussen, J. Nygård, K. Flensberg, and L. P. Kouwenhoven, *Reviews of Modern Physics* **87**, 703 (2015).
- [2] J. Gramich, A. Baumgartner, and C. Schönenberger, *Physical Review Letters* **115**, 216801 (2015).
- [3] A. Benyamini, A. Hamo, S. V. Kusminskiy, F. von Oppen, and S. Ilani, *Nature Physics* **10**, 151 (2014).
- [4] M. M. Shulaker, G. Hills, N. Patil, H. Wei, H.-Y. Chen, H.-S. P. Wong, and S. Mitra, *Nature* **501**, 526 (2013).
- [5] H. Aurich, A. Baumgartner, F. Freitag, A. Eichler, J. Trbovic, and C. Schönenberger, *Applied Physics Letters* **97**, 153116 (2010).
- [6] S. Sahoo, T. Kontos, J. Furer, C. Hoffmann, M. Gräber, A. Cottet, and C. Schönenberger, *Nature Physics* **1**, 99 (2005).
- [7] C. Schönenberger, A. Bachtold, C. Strunk, J.-P. Salvetat, and L. Forró, *Applied Physics A* **69**, 283 (1999).
- [8] L. Langer, V. Bayot, E. Grivei, J.-P. Issi, J. P. Heremans, C. H. Olk, L. Stockman, C. Van Haesendonck, and Y. Bruynseraede, *Physical Review Letters* **76**, 479 (1996).
- [9] M. Bockrath, D. H. Cobden, J. Lu, A. G. Rinzler, R. E. Smalley, L. Balents, and P. L. McEuen, *Nature* **397**, 598 (1999).
- [10] J. Klinovaja and D. Loss, *Physical Review Letters* **110**, 126402 (2013).
- [11] Y. Miyamoto, S. Saito, and D. Tománek, *Physical Review B* **65**, 041402 (2001).
- [12] W. G. van der Wiel, S. De Franceschi, J. M. Elzerman, T. Fujisawa, S. Tarucha, and L. P. Kouwenhoven, *Reviews of Modern Physics* **75**, 1 (2002).
- [13] A. K. Hüttel, S. Ludwig, H. Lorenz, K. Eberl, and J. P. Kotthaus, *Physica E: Low-dimensional Systems and Nanostructures* **34**, 488 (2006).
- [14] T. H. Oosterkamp, T. Fujisawa, W. G. van der Wiel, K. Ishibashi, R. V. Hijman, S. Tarucha, and L. P. Kouwenhoven, *Nature* **395**, 873 (1998).
- [15] M. Jung, J. Schindele, S. Nau, M. Weiss, A. Baumgartner, and C. Schönenberger, *Nano Letters* **13**, 4522 (2013).
- [16] M. R. Gräber, W. A. Coish, C. Hoffmann, M. Weiss, J. Furer, S. Oberholzer, D. Loss, and C. Schönenberger, *Physical Review B* **74**, 075427 (2006).
- [17] S. Sapmaz, C. Meyer, P. Beliczynski, P. Jarillo-Herrero, and L. P. Kouwenhoven, *Nano Letters* **6**, 1350 (2006).
- [18] M. R. Buitelaar, J. Fransson, A. L. Cantone, C. G. Smith, D. Anderson, G. A. C. Jones, A. Ardavan, A. N. Khlobystov, A. A. R. Watt, K. Porfyrakis, et al., *Physical Review B* **77**, 245439 (2008).
- [19] H. W. Liu, T. Fujisawa, Y. Ono, H. Inokawa, A. Fujiwara, K. Takashina, and Y. Hirayama, *Physical Review B* **77**, 073310 (2008).
- [20] A. C. Johnson, J. R. Petta, C. M. Marcus, M. P. Hanson, and A. C. Gossard, *Physical Review B* **72**, 165308 (2005).
- [21] E. A. Laird, F. Pei, and L. P. Kouwenhoven, *Nature Nanotechnology* **8**, 565 (2013).
- [22] L.-J. Wang, G.-P. Guo, D. Wei, G. Cao, T. Tu, M. Xiao, G.-C. Guo, and A. M. Chang, *Applied Physics Letters* **99**, 112117 (2011).
- [23] S. Datta, S. Wang, C. Tilmaciu, E. Flahaut, L. Marty, M. Grifoni, and W. Wernsdorfer, *Physical Review B* **84**, 035408 (2011).
- [24] S. Moon, W. Song, J. S. Lee, N. Kim, J. Kim, S.-G. Lee, and M.-S. Choi, *Physical Review Letters* **99**, 176804 (2007).
- [25] K. Goß, M. Leijnse, S. Smerat, M. R. Wegewijs, C. M. Schneider, and C. Meyer, *Physical Review B* **87**, 035424 (2013).
- [26] S.-H. Kang, G. Kim, and Y.-K. Kwon, *Physical Chemistry Chemical Physics* **17**, 5072 (2015).
- [27] J. Samm, J. Gramich, A. Baumgartner, M. Weiss, and C. Schönenberger, *Journal of Applied Physics* **115**, 174309 (2014).
- [28] T. Hasler, M. Jung, V. Ranjan, G. Puebla-Hellmann, A. Wallraff, and C. Schönenberger, *Physical Review Applied* **4**, 054002 (2015).
- [29] J. J. Viennot, J. Palomo, and T. Kontos, *Applied Physics Letters* **104**, 113108 (2014).
- [30] J. Gramich, A. Baumgartner, M. Muoth, C. Hierold, and C. Schönenberger, *physica status solidi (b)* **252**, 2496 (2015).
- [31] J.-W. Huang, C. Pan, S. Tran, B. Cheng, K. Watanabe, T. Taniguchi, C. N. Lau, and M. Bockrath, *Nano Letters* **15**, 6836 (2015).
- [32] A. Baumgartner, G. Abulizi, K. Watanabe, T. Taniguchi, J. Gramich, and C. Schönenberger, *Applied Physics Letters* **105**, 023111 (2014).
- [33] X. Li, W. Cai, J. An, S. Kim, J. Nah, D. Yang, R. Piner, A. Velamakanni, I. Jung, E. Tutuc, et al., *Science* **324**, 1312 (2009).
- [34] J.-N. Longchamp, C. Escher, and H.-W. Fink, *Journal of Vacuum Science & Technology B* **31**, 020605 (2013).
- [35] L. P. Kouwenhoven, D. G. Austing, and S. Tarucha, *Reports on Progress in Physics* **64**, 701 (2001).
- [36] S. G. Lemay, J. W. Janssen, M. van den Hout, M. Mooij, M. J. Bronikowski, P. A. Willis, R. E. Smalley, L. P. Kouwenhoven, and C. Dekker, *Nature* **412**, 617 (2001).
- [37] J. Cao, Q. Wang, and H. Dai, *Nature Materials* **4**, 745 (2005).